Preprints.org

Article

Empirical Modal Analysis of a Stationary Tail-Rotor Blade of the Bell UH-1H Iroquois "Huey" Military Helicopter Augmented by Operational Structural Dynamics Modification

Daniel Winarski [*] , Marc Lamparelli , Keith Landry , Tyson Winarski

Article

Empirical Modal Analysis of a Stationary Tail-Rotor Blade of the Bell UH-1H Iroquois "Huey" Military Helicopter Augmented by Operational Structural Dynamics Modification

Daniel Winarski [1,*], Marc Lamparelli [2], Keith Landry [3] and Tyson Winarski [4]

[1] Independent Researcher, Tucson, AZ 85710 USA

[2] Technical Support for Spectral Dynamics, Troy, MI 48098, USA

[3] Independent Researcher, Savannah, GA 31405, USA

[4] Sandra Day O'Conner College of Law, Phoenix Campus, Arizona State University, Phoenix, AZ 85004, USA

* Correspondence: winarskifirm@gmail.com

Abstract

In the multi-degree of freedom portion of the undergraduate vibrations engineering course taught at the United States Military Academy and West Point, New York, instructors ask the students (a) how we identify system parameters of effective mass and/or mass moment of inertia, stiffness, and damping as well as (b) whether our implicit assumption, that these properties were constant for systems in motion, was valid. Instructors then use concepts from several other engineering courses along with an introduction to experimental methods to answer these questions. One set of answers to these questions came from the analysis of the elastic vibration of a tail-rotor blade from a U.S. Army UH-1H "Huey" helicopter. This analysis required the integration of fields of vibrations engineering with dynamics and mechanics of materials. Use of modal analysis empirically determined three out-of-plane flapping modes as well a torsional mode of vibration for a nonrotating blade. For this modal analysis, a Brüel and Kjær 2034 signal analyzer was used to gather frequency response functions of the stationary rotor blade as excited by an impact hammer. The response to the excitation was measured with an accelerometer. The centrifugal-stiffening effect of the operational angular velocity of the rotor blade was simulated via structural dynamics modification. This problem presented many interesting challenges and provided an innovative means of coupling material from different undergraduate courses to solve a real-world engineering problem.

Keywords: helicopter; tail-rotor blade; modal analysis; structural dynamics modification; centrifugal-stiffening

1. Introduction

There is a long history of helicopter vibration studies. Nygren [1] investigated helicopter higher harmonic control using a dynamic system coupler simulation for his Ph.D. dissertation. He also published a test plan using the Langley Rotorcraft Structural Dynamics Program to develop an efficient means of coupling a main rotor to the airframe [2]. Additionally, Nygren and Schrage studied fixed-gain versus adaptive higher harmonic control simulation [3]. Grappasonni, et-al., [4] studied the vibrations in a Lynx Mk7 airframe and an AgustaWestland lightweight helicopter tail frame without the tail-rotor. Results were quantified via Modal Assurance Criterion diagrams. Rizo-Patron and Sirohi studied the theoretical and empirical modal analysis of the first three out-of-plane flapping modes of a beam simulating a helicopter rotor, using digital image correlation as the beam rotated at 0, 300, 600, and 900 RPM [5]. Torsion was not studied. This paper included a centrifugal stiffening term which involved mass per unit length and the square of Ω, the speed of rotation. Pierro,

et-al., studied the vibro-acoustical operational modal analysis of a helicopter cabin [6]. Agneni, et-al., studied the output-only modal analysis of a rotating helicopter blade in the German Aerospace Center [7]. Ameri, et-al., conducted ground vibration tests of a helicopter frame [8]. Sibille, et-al., investigated the automated operational modal analysis of a Airbus Helicopter H135 bearingless main rotor blade with a density-based cluster algorithm [9].

Češkovič, et-al., investigated unwanted supplementary vibrations of helicopter radio communication systems [10]. Tamer, Aet-al., focused on a generalized index for the assessment of helicopter pilot vibration exposure [11]. Chiariello, et-al., published their results on the vibration qualification campaign on the main landing gear system for a high-speed compound helicopter [12]. Yang, et-al., reduced helicopter vibration loads by individual blade control with a genetic algorithm [13]. Bertolino, et-al., developed of a high-performance low-weight hydraulic damper for active vibration control of the main rotor on helicopters [14,15]. Wang, et-al., evaluated a topological valley stamping plate for low-frequency-vibration isolation and wave manipulation in helicopters [16]. Tamer, et-al., studied cabin layout optimization for vibration hazard reduction in helicopter emergency medical service [17]. Feng [18] developed a method of eliminating helicopter vibration interference magnetic field with a pair of magnetometers. Our study differed from these by our constructing a stationary model of a helicopter tail-rotor blade using the STAR7 software from Spectral Dynamics. Then we augmented this stationary model to an operational rotating velocity via use of the STAR7 Structural Dynamics Modification.

2. Modal Measurements at the United States Military Academy, West Point

The Bell UH-1 Iroquois (nicknamed "Huey") [19] was the beginning of a family of utility military helicopters designed and produced by the American aerospace company Bell Helicopter. It was also the first turbine-powered helicopter in service with the United States military.

Figure 1 shows a Bell UH-1H Iroquois along with the X- and Z-axes used in the coordinate system of this study. This aircraft has a maximum gross weight of 9,500 lbs., a cruise speed of 90 knots, and a maximum speed of 120 knots. It was a tail-rotor blade of this model of helicopter which was loaned for this study by the Second Aviation Detachment stationed at the Steward Army Air Field, Newburgh, New York.


Figure 1. Bell UH-1H Iroquois [20] with Coordinate System.

The tail-rotor of the UH-1H helicopter had two blades. The radius R of the arc of the tail-rotor was 1.295 meters (4.25 feet). Its operational angular velocity was Ω_z=173.2 radians/second (1,654 RPM) about the horizontal Z-Axis. The Y-Axis chord of the largely rectangular blade was 213.6 mm (8.41 inches). The mass of the one blade was approximately 3 kg and the overall blade length along

the X-Axis was L=1.16 meters. The center of mass was located 0.685 meters from the outer edge, 0.475 meters from the inner edge of the blade. Two mount holes, 30 mm from the root end of the blade, were used to cantilever the tail-rotor blade from a steel channel, as shown in Figure 2.

The empirical modal analysis of one tail-rotor of a Bell UH-1H Iroquois "Huey" military helicopter was done in lab D-18, Mahan Hall, the United States Military Academy at West Point, New York. Figure 2 shows the layout of 45 nodes along the top surface of the UH-1H tail-rotor blade, which is effectively a fixed-free cantilever beam. A Brüel & Kjær 4393 Accelerometer (fixed-location response, in m/s^2) [21] was mounted at the radially outermost node along the trailing edge of the tail-rotor blade (node 16), Figure 2, with beeswax. It was felt that measuring the system response at this node would afford the maximum sensitivity to both flapping and torsion and would not be a vibrational node (point of zero amplitude for any of the modal resonances). The end view of the tail-rotor blade in Figure 2 was photographed at the Pima Air and Space Museum, [22]. This blade rotated clockwise about the Z-axis.
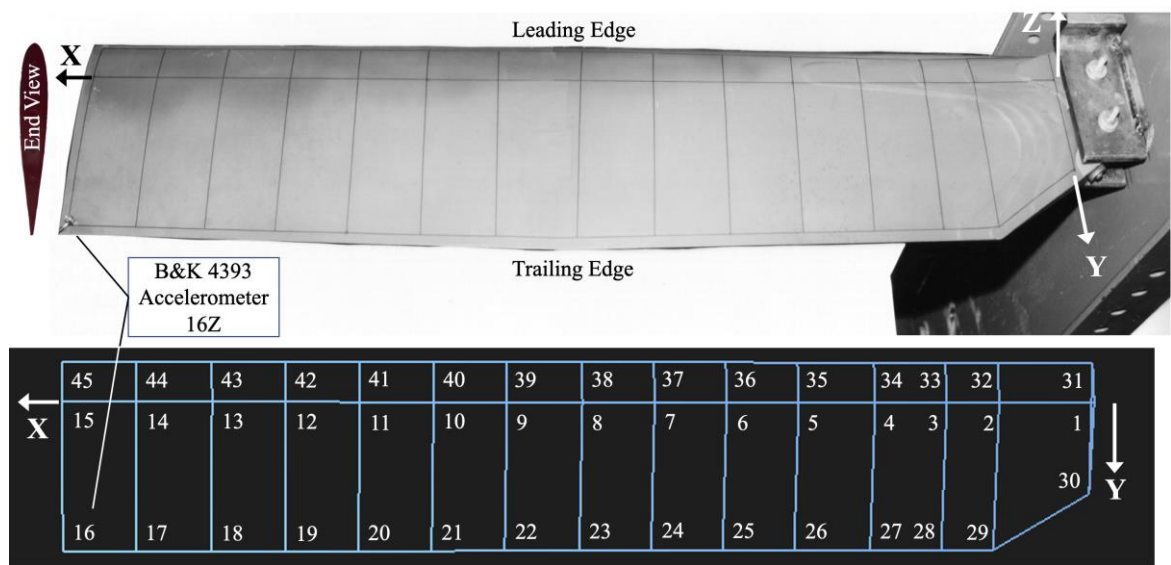
Figure 2. Layout of 45 Nodes along the Top Surface of the UH-1H Tail-Rotor Blade.

As shown in Figure 3, a Brüel & Kjær 8202 impact hammer and 8200 force transducer (excitation, in Newtons) [23] were used to gently tap the 45 nodes, and the fixed location Brüel & Kjær 4393 accelerometer sensed the subsequent response. Using the hard-rubber tip, without the additional mass, on the 8202 impact hammer limited the excitation to 500Hz, coinciding nicely with the 400Hz bandwidth on the Brüel & Kjær 2034 Analyzer. Brüel & Kjær 2644 line-driver charge-amplifiers [24] amplified the low-level signals from the 4393 accelerometer and 8200 force transducer before these signals were received by the Brüel & Kjær 2034 signal analyzer. The outputs of the Brüel & Kjær 2034 signal analyzer were 45 Frequency Response Functions (*.FRF). Structural Measurements System (SMS) StarStruc software originally performed the calculation of mode shapes, modal frequency and modal damping ratios, similar to that described by Winarski [25].
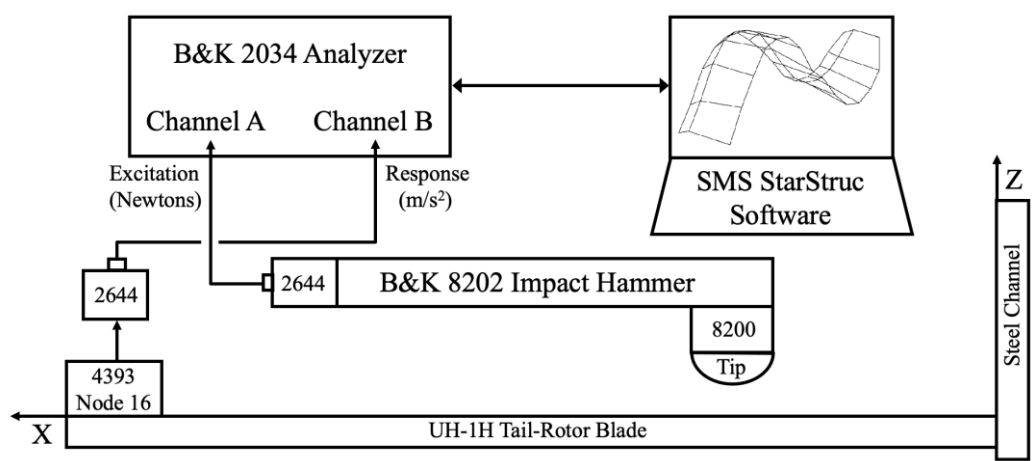
Figure 3. Diagram of Experimental Setup.

Table 1 lists the XYZ coordinates of the 45 nodes comprising the helicopter tail-rotor blade. The nodes were numbered starting along the thickest portion of the blade, then along the trailing edge of the blade, then finally along the leading edge of the blade.

Table 1. 45 Star7 Modal Nodes comprising the Helicopter Tail-Rotor Blade.

Star7 Node	X (m)	Y (m)	Z (m)	Rotor Blade Component	Star7 Node	X (m)	Y (m)	Z (m)	Rotor Blade Component
1	0	0	0.02	Max Thick	2	0.10	0	0.02	Max Thick
3	0.16	0	0.02	Max Thick	4	0.23	0	0.02	Max Thick
5	0.31	0	0.02	Max Thick	6	0.38	0	0.02	Max Thick
7	0.46	0	0.02	Max Thick	8	0.54	0	0.02	Max Thick
9	0.61	0	0.02	Max Thick	10	0.69	0	0.02	Max Thick
11	0.76	0	0.02	Max Thick	12	0.84	0	0.02	Max Thick
13	0.92	0	0.02	Max Thick	14	1.00	0	0.02	Max Thick
15	1.07	0	0.02	Max Thick	16	1.07	0.16	0	B&K 4393
17	1.00	0.16	0	Trailing	18	0.92	0.16	0	Trailing
19	0.84	0.16	0	Trailing	20	0.76	0.16	0	Trailing
21	0.69	0.16	0	Trailing	22	0.61	0.16	0	Trailing
23	0.54	0.16	0	Trailing	24	0.46	0.16	0	Trailing
25	0.38	0.16	0	Trailing	26	0.31	0.16	0	Trailing
27	0.23	0.16	0	Trailing	28	0.16	0.16	0	Trailing
29	0.10	0.16	0	Trailing	30	0.00	0.10	0	Trailing
31	0	−0.04	0	Leading	32	0.10	−0.04	0	Leading
33	0.16	−0.04	0	Leading	34	0.23	−0.04	0	Leading
35	0.31	−0.04	0	Leading	36	0.38	−0.04	0	Leading
37	0.46	−0.04	0	Leading	38	0.54	−0.04	0	Leading
39	0.61	−0.04	0	Leading	40	0.69	−0.04	0	Leading
41	0.76	−0.04	0	Leading	42	0.84	−0.04	0	Leading
43	0.92	−0.04	0	Leading	44	1.00	−0.04	0	Leading
45	1.07	−0.04	0	Leading					

3. Transferring Modal Measurements from SMS StarStruc to Spectral Dynamics STAR7

Eventually, this StarStruc software became obsolete. After much detective work, it was determined that GenRad had acquired Structural Measurements System, then Spectral Dynamics had acquired GenRad. Spectral Dynamics took a special interest in advancing this project, including instructions on how to import the old SMS *.CRD coordinate file and the 45 old SMS *.FRF Frequency Response Function files into their latest STAR7 Premier Modal software 3410-9710 [26], as summarized in Figure 4. The old SMS *.DSQ display sequence did not require separate importing.

The transfer of modal results from the old SMS StarStruc package to the new Spectral Dynamics STAR7 package began with creating a workspace then creating a project within that workspace. Once inside that project, as shown in Figure 4, right click on MODEL > IMPORT and select STAR v5 Coordinate Tables (*.CRD). Navigate to the desired SMS *.CRD file and upload it, to produce the basic geometry of the modal analysis. Next, right click on MEASUREMENT DATA > IMPORT and select STAR v5 Measurements. Navigate to the desired SMS *.FRF files, select all using shift-click, and upload them. Lastly, open PARAMETERS and select the units of SI HZ, Excitation in Newtons for the Brüel & Kjær 8202 impact hammer and 8200 force transducer, and Response in m/s^2 for the Brüel & Kjær 4393 accelerometer. Under acquisition setup, Fixed Response was selected, and the master reference was 16Z as the 4393 accelerometer was at node 16 in the Z direction. Using the FILE menu, the project was then saved as a new *.PRJ file in the respective *.SWS workspace file, resulting in the model being saved to a new *.CMM file and the measurements being saved to a new *.SDD file.
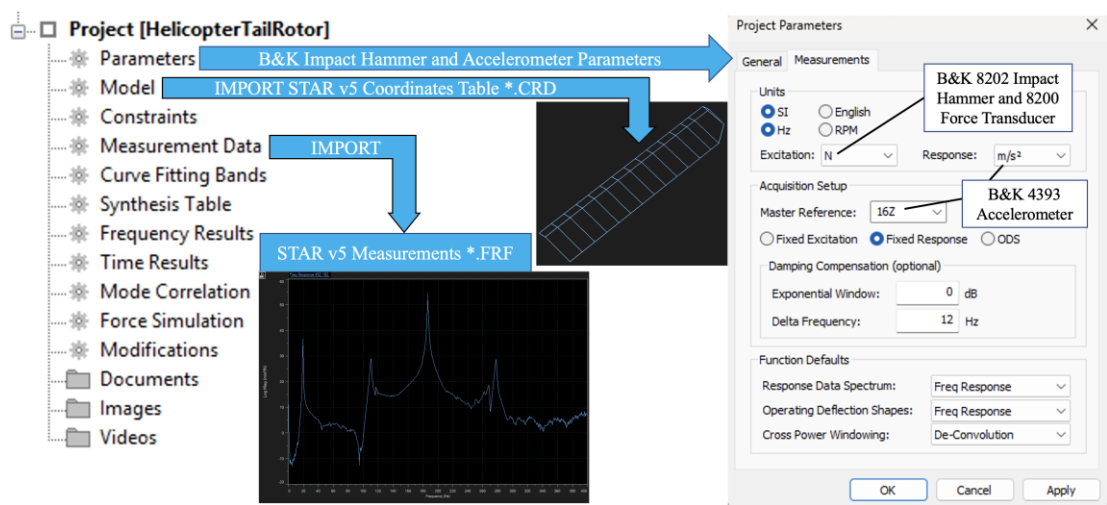

**Figure 4.** Transfer from old SMS StarStruc package to the new Spectral Dynamics STAR7.

4. Identifying Modes of Vibration Using STAR7

Figure 5 shows the exemplary 45Z-16Z Frequency Response Function displaying four potential modes of vibration over the frequency range of $0 \leq \omega \leq 400Hz$. 45Z-16Z meant that this was the response at node 45Z with the reference at 16Z, the location of the Brüel & Kjær 4393 accelerometer. 45Z was picked as the exemplary response because it was at the outer extremity of the rotor and at the leading edge of the rotor blade. With the 4393 accelerometer at the outer extremity of the rotor and at the trailing edge of the rotor blade, it was felt that the 45Z-16Z pair gave the best representation of both the flapping and torsional modes of vibration of the subject rotor blade.
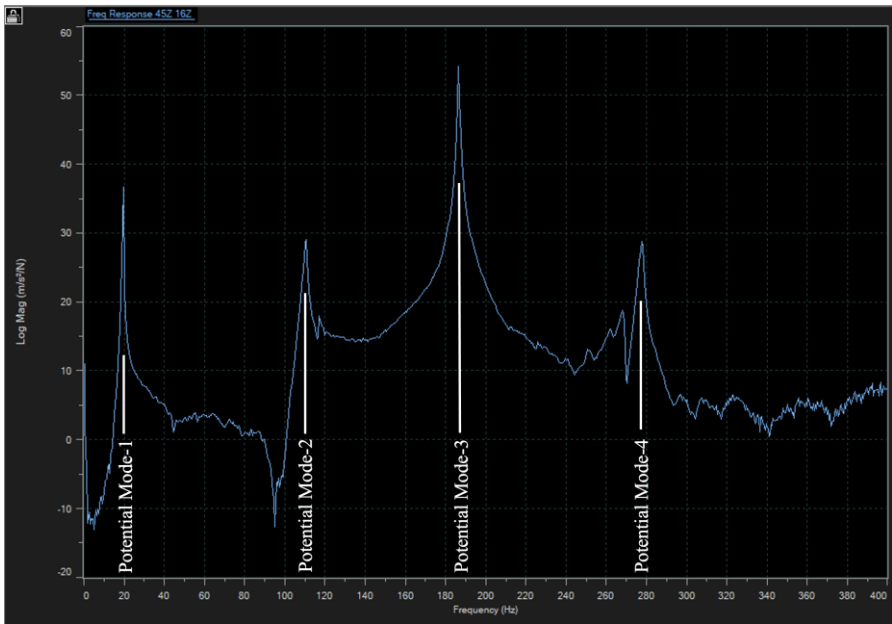
Figure 5. 45Z-16Z Frequency Response Function displaying four potential modes.

The mode identification using the Advanced Curve Fitter method began by selecting Analysis from the top tool bar, then selecting Mode Indicators for all 45 nodes. The creation of the normal (normalized between 0 and 1 as shown on the vertical axis) Mode Indicator Function (MIF) is shown as the blue line in Figure 6.
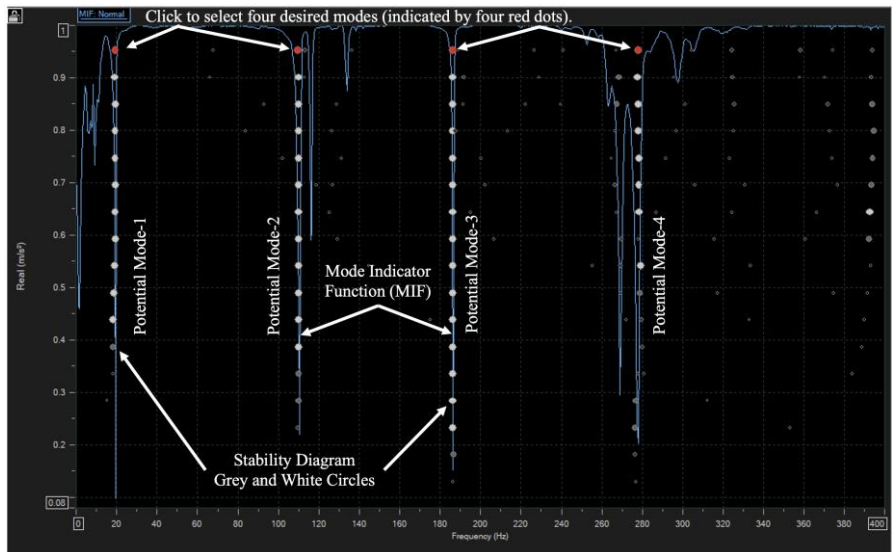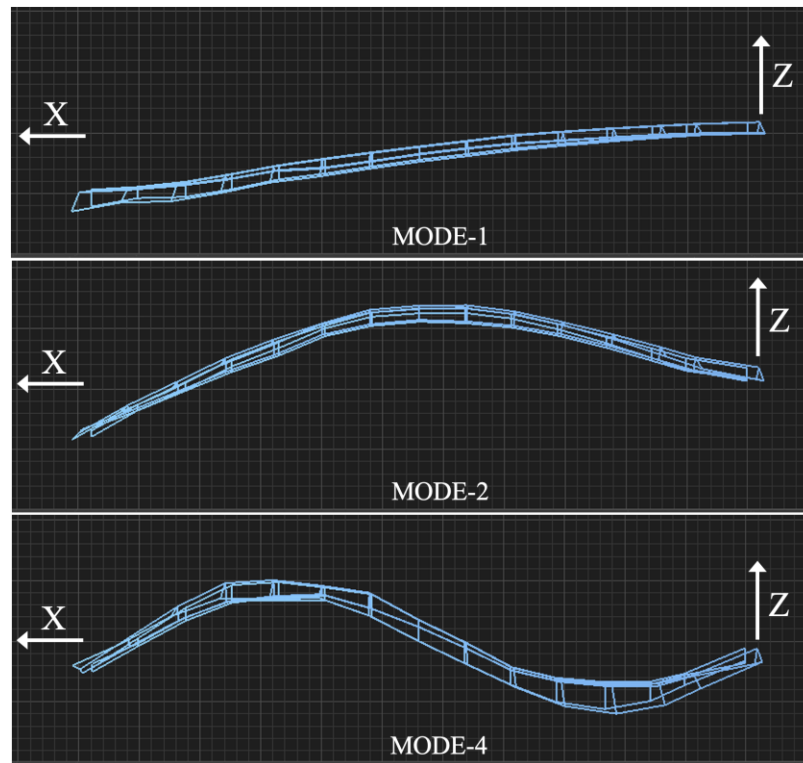

Figure 6. Advanced Curve Fitter Method showing Mode Indicator Function.

Next, the Stability Diagram icon was selected, to superimpose the circles of the Stability Diagram upon the Mode Indicator function in Figure 5. From the Estimate FD tab, select Model Size from 4 to 20 and click Calculate. If a potential mode was found, the Stability Diagram reported an open circle. If the same mode was stable within the frequency tolerance, a light gray circle was reported. If both the difference in frequency and damping values were within tolerance, the new circle was shaded light gray. If both the difference in frequency and damping values were in tolerance, the new circle was shaded dark gray. If the frequency and damping values were again in tolerance, the new circle was shaded white. A progression of dark grey circles followed by white circles was clearly evident in Figure 6. In order to calculate the four mode shapes seen in Figures 7-8, each mode had to be

selected by clicking on one of the circles, as shown by the four red circles, then selecting Analysis > Curve Fitting > Poly-Reference and clicking on Fit All.

5. Output of STAR7

Figure 7 shows flapping modes 1, 2, and 4 from the perspective of the X-Z plane, which best differentiates between the three distinctive mode shapes for a nonrotating tail-rotor blade, $\Omega_z=0$.

Figure 7. Flapping Modes 1, 2 and 4, using the Advanced Curve Fitter method, $\Omega_z=0$.

Figure 8 then shows an isometric view of torsional mode-3, to better visualize the rotational-deflection of the nonrotating tail-rotor blade about the X-axis.
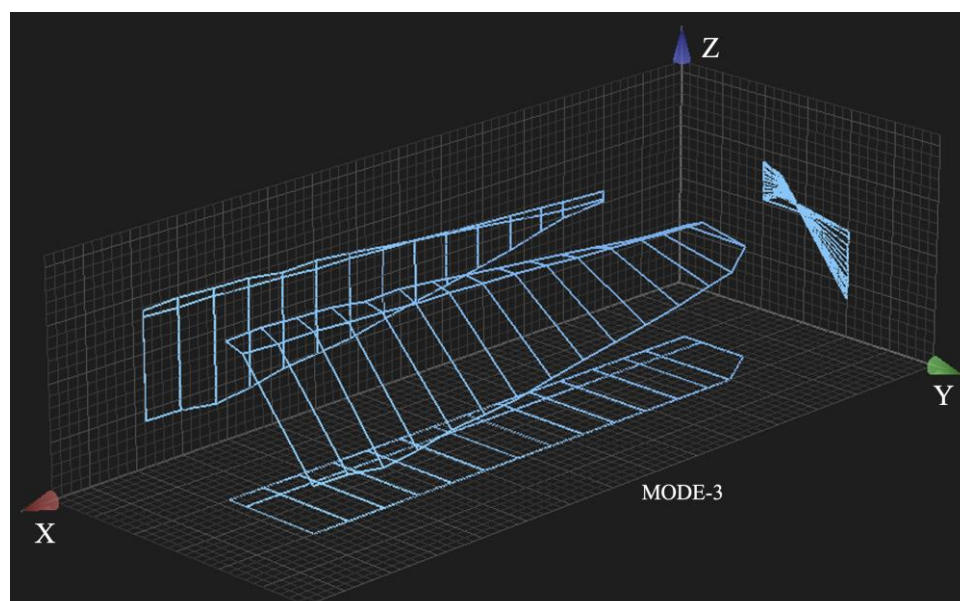
Figure 8. Torsion Mode-3 using the Advanced Curve Fitter method, $\Omega_z=0$.

The information from Figures 7-8 is summarized in Table 2, where the modes are numbered in order of frequency. The frequencies and damping determined by STAR7-ACF were very close to the previous SMS StarStruc software values obtained using the polynomial method.

Table 2. Star7 and SMS StarStruc Empirical Modal Frequencies and Damping, Ω_z=0.

Star7 Mode Number	Star7-ACF Mode Type	Star7-ACF Frequency ω	Star7-ACF Damping ζ	StarStruc Frequency ω	StarStruc Damping ζ
1	Flapping	19.32 Hz	1.51 %	19.68 Hz	0.46 %
2	Flapping	109.78 Hz	1.00 %	111.27 Hz	0.26 %
3	Torsion	186.44 Hz	0.20 %	186.56 Hz	0.13 %
4	Flapping	278.11 Hz	0.62 %	278.24 Hz	0.36 %

Table 3 lists the empirical frequency ratios in column 3 for the three STAR7 flapping frequencies in column 2, from Table 2. The ratio of 5.68:1 was calculated from the quotient 109.78/19.32, and the ratio of 14.39:1 was calculated from the quotient 278.11/19.32.

Table 3. Comparing Star7 Flapping Frequencies, for Ω_z=0.

Star7 Flapping Mode	Star7-ACF Frequency ω	Star7 Frequency Ratio	Blevins Ratio [27]	Yoo and Shin Ratio [28]	Wright, et-al. Ratio [29]	Lima Ratio [30]
1 (Table 2)	19.32 Hz	1 : 1	1 : 1	1:1	1:1	1:1
2 (Table 2)	109.78 Hz	5.68 : 1	6.267 : 1	6.267 : 1	6.267 : 1	6.267 : 1
4 (Table 2)	278.11 Hz	14.39 : 1	17.547 : 1			17.547 : 1

In column 4 of Table 3, the corresponding theoretical frequency ratios were listed from Blevins [27], for an Euler-Bernoulli beam of uniform cross-section. In column 4, the ratio of 6.267:1 was calculated from $(\lambda_2/\lambda_1)^2$, where λ_2=4.69409113 and λ_1=1.87510407. Similarly, the ratio of 17.547:1 was calculated from $(\lambda_3/\lambda_1)^2$, where λ_3=7.85475744.

In columns 5-7 of Table 3, the corresponding theoretical frequency ratios were listed from Yoo and Shin [28], Wright, et-al., [29], and Lima [30], respectively. Columns 4-7 indicated a reasonable agreement between the published Euler-Bernoulli theory and the experimental results from the tail-rotor blade using STAR7, as tabulated in column 3. The =PEARSON correlation between the STAR7 frequency ratios in column 3 of Table 3 and the Blevins frequency ratios in column 4 and Lima ratios in column 7 was 99.9%, indicating a very strong correlation between our stationary tailrotor blade and a stationary Euler-Bernoulli beam.

6. STAR7 Modal Assurance Criterion, Ω_z=0

In Figure 9, the 3-D histogram (left) and 2-D table (right) Modal Assurance Criterion [31] for the STAR7 Advanced Curve Fitter are displayed for the four modes of vibration of interest shown in Figures 7-8, at Ω_z=0. Pastor [32] was helpful in understanding Figure 9.

In Figure 9, the MAC is a symmetric 4-by-4 matrix calculated by the dot product of eigenvectors of pairs of the four subject modes. The comparison values for each pair of modes varied between 0 and unity (100%). The main-diagonals in Figure 9 represented a form of autocorrelation and all were unity, as expected. A form of cross-correlation is shown for half of the off-diagonal elements (6 total) is depicted via a histogram then tabulated for all off-diagonal elements (12 total).

The color coding for Figure 9 was as follows: purple represented a value between 0.90 (90%) and 1.00 (100%) as used for the main-diagonal values, burnt-orange represented a value between 0.50 (50%) and 0.90 (90%), pink represented a value between 0.02 (2%) and 0.50 (50%) as used for several off-diagonal values, and yellow-lime represented a value between 0 (0%) and 0.02 (2%) as used for

several off-diagonal values. The low off-diagonal values in Figure 9 indicated a high degree of orthogonality between modes 1-4, as desired.
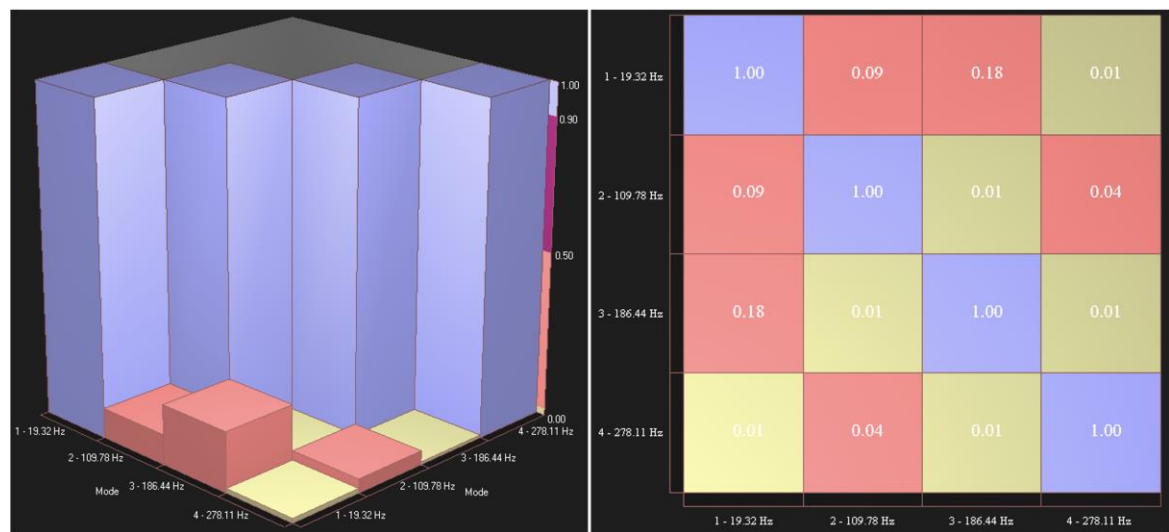

Figure 9. 3-D histogram (left) and 2-D table (right) Modal Assurance Criterion, Ω_z=0.

7. STAR7 Structural Dynamics Modification: DOF-to-Ground for Ω_z=173.2 rad/sec

The STAR7 DOF-to-ground structural dynamics modification [30] was chosen to add stiffness to the tail-rotor blade. This simulated the centrifugal stiffening caused by the rotation of the blade when in operation at Ω_z=173.2 radians/second (1,652 RPM), Table 4.

Assuming a nodal mass of m=60 grams across all 45 nodes gave a spring rate in the Z direction of $K_z=m\Omega_z^2$=1800N/m. The nodal mass of m=60g gave a mass of 2.7kg (45 times 0.06), which allowed about 0.3kg for the attachment stem at the base of the blade. Each DOF-to-ground connection was made using the entries in Table 4, specifying the use of spring modifications via N/m in column 3, the actual stiffness (spring rate) desired which was 1800N/m in column 4, the degree of freedom to be stiffened in the Z out-of-plane direction in column 5, the other end of the spring being attached to ground in column 6, and the default values of ground to be (X,Y,Z) = (0,0,0) in columns 7-9.

Spring rates in the Z direction were calculated as $K_z=m\Omega_z^2$ N/m. The Z-axis was chosen for the DOF-to-ground structural dynamics modification because all four modes of vibration consisted of out-of-plane Z-axis motion. Figure 7 clearly showed that the flapping modes 1, 2, and 4 had their displacements in the Z-direction. Although Figure 8 showed that the torsion mode-3 rotated about the X-axis, this torsion mode comprised the leading edge of the tail-rotor blade displacing in one Z-axis direction and the trailing edge of the tail-rotor blade displacing in the opposite Z-axis direction. Thus, all four subject modes involved Z-axis motion.

Table 4. STAR7 Structural Dynamics Modification Table, Ω_z=173.2 rad/sec.

Row	Enable	Type	Amount	DOF/Point 1	DOF/Point 2	Ground X	Ground Y	Ground Z
1	✓	N/m	1800	1Z	GROUND	0	0	0
2	✓	N/m	1800	2Z	GROUND	0	0	0
3	✓	N/m	1800	3Z	GROUND	0	0	0
...	...	...	...	...	...	...	...	...
45	✓	N/m	1800	45Z	GROUND	0	0	0

Table 5 first lists the STAR7 frequency and damping for modes 1-4, at zero angular velocity, as previously listed in Table 2. Modes 5-8 are modes 1-4 respectively, with structural dynamics

modification (SDM), specifically springs specified in Table 4 which were designed to simulate centrifugal stiffening that tended to straighten the helicopter tail-rotor blade and raise modal frequencies when at its operational angular velocity of 173.2 radians per second.

Table 5. STAR7 Empirical Modal Frequencies and Damping, Ω_z=0 and 173.2 rad/sec.

Star7 Mode Number	Angular Velocity Ω_z	Star7-ACF Frequency ω	Star7-ACF Damping ζ
1 (Source: Table 2)	0	19.32 Hz	1.51 %
2 (Source: Table 2)	0	109.78 Hz	1.00 %
3 (Source: Table 2)	0	186.44 Hz	0.20 %
4 (Source: Table 2)	0	278.11 Hz	0.62 %
5 (Mode-1 + SDM)	173.2	36.26 Hz	0.81 %
6 (Mode-2 + SDM)	173.2	114.41 Hz	0.96 %
7 (Mode-3 + SDM)	173.2	190.90 Hz	0.19 %
8 (Mode-4 + SDM)	173.2	279.60 Hz	0.61 %

Yoo and Shin [28] and Lima [30] defined the important constant T, which is the reciprocal of the square root used by Blevins [27]. T has the units of seconds.

$$T = \sqrt{\frac{ML^4}{EI}} = \frac{1.87510407^2}{2\pi(19.32)} = 0.028964 \; seconds$$

Yoo and Shin [28] and Lima [30] then defined the nondimensional rotational velocity used to calculate γ=5.017, which is the product of T and Ω_z=173.2 radians/second.

$$\gamma = T\Omega = 5.017$$

This nondimensional rotational velocity was critical for calculating the flapping frequency ratios of 1.839:1 (between mode-5 and mode-1) and 1.156:1 (between mode-6 and mode-2) from both Yoo and Shin [28] and Wright, et-al. [29], as represented in columns 5-6 in Table 6. The value of 1.839:1 was very close to the STAR7 value of 1.877:1, when comparing mode-5 (mode-1 with SDM) and mode-1 itself. The value of 1.059:1, when comparing mode-8 (mode-4 with SDM) and mode-4 itself, was inferred from Figure 2 of Yoo and Shin [28].

Table 6. Flapping Frequency Ratios, for Ω_z=173.2 vs Ω_z=0 rad/sec.

Star7 Flapping Mode	Star7-ACF With SDM Ω_z=173.2	Star7-ACF Stationary Ω_z=0	Ω_z=173.2 Vs Ω_z=0 Ratio	Yoo and Shin Ratio, γ=5.017 [28]	Wright Ratio, γ=5.017 [29]
5 (1+SDM)	36.26 Hz	19.32 Hz	1.877 : 1	1.839 : 1	1.839 : 1
6 (2+SDM)	114.41 Hz	109.78 Hz	1.042 : 1	1.156 : 1	1.156 : 1
8 (4+SDM)	279.60 Hz	278.11 Hz	1.005 : 1	1.059 : 1	

Figure 10 and Table 6 show the following. The STAR7 SDM model of the helicopter tail-rotor blade shows that the ratios between the operational (Ω_z=173.2 rad/sec) versus stationary (Ω_z=0) decrease with increasing flapping mode. All three modes showed all frequency ratios exceed 1:1 indicating centrifugal-stiffening. Additionally, the STAR7 SDM model slightly exceeded Yoo and Shin [28], and Wright [29] for the first flapping ratio, mode-5:mode-1. However, the STAR7 SDM model was slightly lower than Yoo and Shin [28] as well as Wright [29] for the second flapping ratio, mode-6:mode-2. Lastly, the STAR7 SDM model was slightly lower than Yoo and Shin [28] for the third flapping ratio, mode-8:mode-4. The =PEARSON correlation between the STAR7 frequency ratios in column 4 of Table 6 and the Yun and Shin frequency ratios in column 5 was 99.7%, indicating

a very strong correlation between our centrifugally-stiffened tailrotor blade and a centrifugally-stiffened Euler-Bernoulli beam.
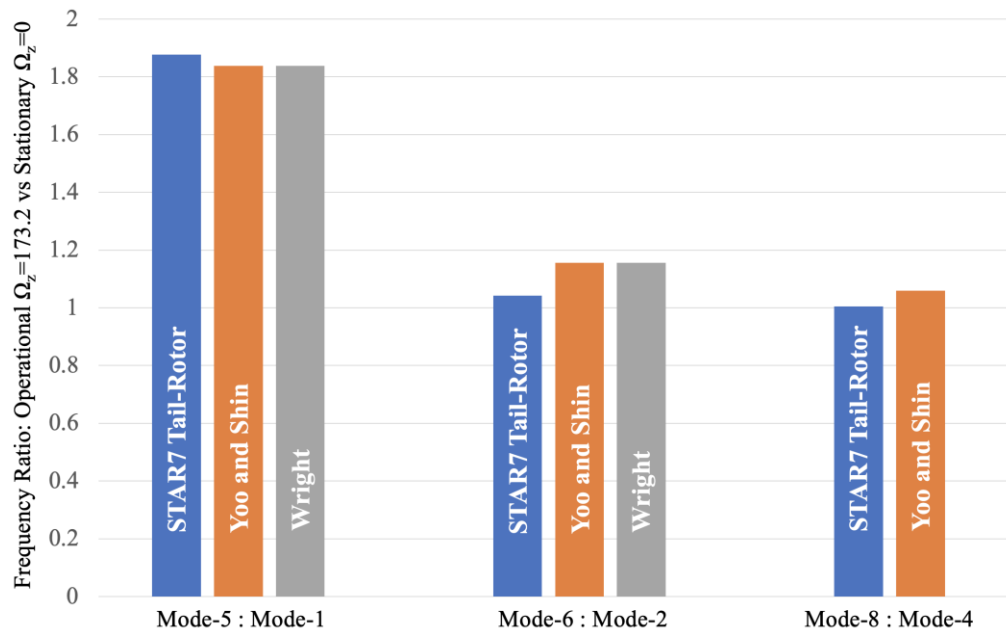
Figure 10. Frequency Ratio: Operational (Ω_z=173.2) versus Stationary (Ω_z=0).

8. STAR7 Combined Modal Assurance Criterion, for Ω_z=0 and Ω_z=173.2 rad/sec

Figure 11 shows a 3-D histogram (left) and a 2-D table (right) Modal Assurance Criterion for Ω_z=0 (modes 1-4) and Ω_z=173.2 rad/sec (modes 5-8, which are modes 1-4 with structural dynamics modification). Auxiliary thick black lines, superimposed on the 8-by-8 MAC table, divided it into four 4-by-4 quadrants. The upper left-quadrant of the 2-D table MAC in Figure 11 represents the apples-to-apples comparison of modes 1-4 for zero angular velocity, Ω_z=0, as previously shown separately in Figure 9. The lower right-quadrant of the 2-D table MAC in Figure 11 is the apples-to-apples comparison of modes 5-8, where modes 1-4 now experience an operational angular velocity of Ω_z=173.2 radians per second. Both the upper-left and the lower-right quadrants are symmetric, and the purple main diagonal which they form has values of 100% for an autocorrelation, as expected. The lower-left and the upper right quadrants of the 2-D table MAC in Figure 1 are apples-to-oranges comparisons of modes 1-4 versus modes 5-8. The lower-left and the upper right quadrants are not themselves symmetric about their respective subdiagonals; however, these two quadrants are mirror-images of each other about the main diagonal of Figure 11. Thus, the overall 8-by-8 MAC in Figure 11 is a symmetric matrix, as desired. Additionally, the purple subdiagonals in the lower-left and the upper right quadrants of the 2-D table MAC showed 100% correlations, indicating that the mode shapes in Figures 7-8 were not meaningfully affected between the stationary angular velocity of Ω_z=0 and the operational angular velocity of Ω_z=173.2 radians per second. Yoo and Shin [28] did report shifts in mode shape, but at the nondimensional rotational velocity of γ=50, which was an order of magnitude greater than our value of γ=5.017.
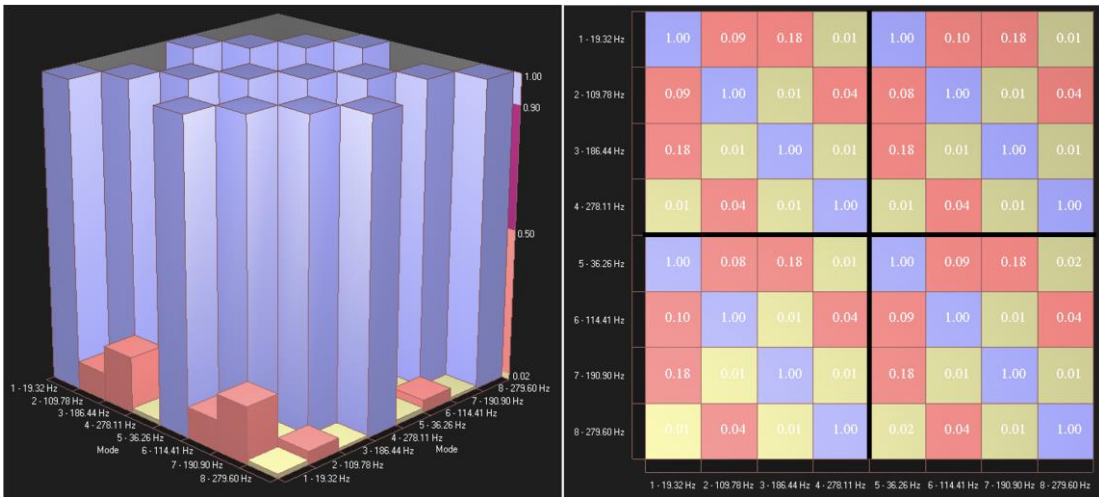
Figure 11. 3-D (left) and 2-D (right) Modal Assurance Criterion, Ω_z=0 and 173.2 rad/sec.

9. Conclusions

To facilitate the understanding of the undergraduate students who have not had courses in helicopter design, the structural modification package of the STAR7 software was used to model the helicopter tail-rotor in its zero angular velocity and its operational mode. In its operational mode, the tail-rotor spins at constant angular velocity Ω_z about the horizontal Z-Axis. This rotational motion stiffens the blade beyond the flexural rigidity taught in mechanics of materials. We showed how to implement structural dynamics modification within the Spectral Dynamics STAR7 software, so that future cadets at the United States Military Academy can simulate different flight conditions once a basic modal model is established at a zero angular velocity within a laboratory.

At the point of manufacture, the frequencies and damping obtained by STAR7 could be blockchained [33] to other manufacturing records, for the purpose of determining when a rotor-blade might need replacement.

This study was limited to the analysis of a helicopter tail-rotor blade. Although highly desired, getting a main rotor blade proved impossible. Additionally, when a helicopter turns, coriolois acceleration is developed, which we did not consider.

Abbreviations

The following abbreviations were used in this manuscript:

2-D   Two dimensional
3-D   Three dimensional
*.CMM   STAR7 model file
*.CRDCoordinates file (SMS StarStruc)
*.DSQDisplay Sequence file (SMS StarStruc)
*.FRF Frequency Response Function file (SMS StarStruc)

*.PRJ　　　　Project file (STAR7)

*.SDD Spectral Dynamics Data file (STAR7)

*.SWS STAR7 workspace file

ACF　　　　Advanced Curve Fitter Method (STAR7)

B&K　　　　Brüel & Kjær, as of 2019 now called HBK (Hottinger Brüel & Kjær)

DOF　　　　Degree Of Freedom

E　　　　Effective Youngs Modulus of Tail-Rotor Blade

EI　　　　Effective Flexural Rigidity of Tail-Rotor Blade

FD　　　　Frequency and Damping

I　　　　Effective Area Moment of Inertia of Tail-Rotor Blade about its Neutral Axis

K_z　　　　STAR7 SDM Stiffness addition, spring rate in the Z direction

L　　　　Length of Tail-Rotor Blade, 1.16m

m　　　　Nodal Mass attributed individually to each of the 45 nodes

M　　　　Mass per unit length of Tail-Rotor Blade

MAC　Modal Assurance Criterion, either a histogram (3-D) or a table (2-D)

MIF　　　　Mode Indicator Function (STAR7)

R　　　　Arc of the tip of Tail-Rotor, 1.295m

RAFA Rotation About a Fixed Axis

SDM　　　　Structural Dynamics Modification

SMS　　　　Structural Measurements System

STAR7　　　　Spectral Dynamics modal analysis software

T　　　　Vibrational constant, with units of seconds

γ　　　　Nondimensional rotational velocity, $\gamma = T\Omega_z$

ζ　　　　Modal Damping Ratio, in Percent

λ　　　　Solutions to the transcendental equation $\cos(\lambda)\cosh(\lambda) + 1 = 0$

ω　　　　Modal Vibration Frequency, in Hertz

Ω_z　　　　Angular velocity in rad/sec of the Tail-Rotor Blade about the Z-axis

References

1.　　Nygren, Kip Peter. "An Investigation of Helicopter Higher Harmonic Control using a Dynamic System Coupler Simulation (Vibrations, Parameter Identification)." PhD diss., Georgia Institute of Technology, 1986, (accessed on 19 July 2025).

2.　　Nygren, Kip P. "Calculation of rotor impedance for use in design analysis of helicopter airframe vibrations." *Hampton Univ., NASA/American Society for Engineering Educ* (1990), (accessed on 19 July 2025).

3.　　Nygren, Kip P., and Daniel P. Schrage. "Fixed-gain versus adaptive higher harmonic control simulation." *Journal of the American Helicopter Society* 34, no. 3 (1989): 51-58, (accessed on 19 July 2025).

4.　　Grappasonni, Chiara, N. Ameri, Giuliano Coppotelli, D. J. Ewins, A. Colombo, E. Bianchi, V. Barraco, and Universit degli Studi di Roma. "Dynamic identification of helicopter structures using operational modal analysis methods in the presence of harmonic loading." In *Proceedings of the ISMA*. 2012, (accessed on 19 July 2025).

5.　　Rizo-Patron, S., and Jayant FSirohi. "Operational modal analysis of a helicopter rotor blade using digital image correlation." *Experimental Mechanics* 57, no. 3 (2017): 367-375, (accessed on 19 July 2025).

6.　　Pierro, Elena, Emiliano Mucchi, L. Soria, and A. Vecchio. "On the vibro-acoustical operational modal analysis of a helicopter cabin." *Mechanical Systems and Signal Processing* 23, no. 4 (2009): 1205-1217, https://doi.org/10.1016/j.ymssp.2008.10.009, (accessed on 20 July 2025).

7.　　Agneni, Alessandro, Giuliano Coppotelli, and Chiara Grappasonni. "Operational modal analysis of a rotating helicopter blade." In *Proceedings of ISMA*, pp. 16-00184. 2010, (accessed on 20 July 2025).

8.　　Ameri, N., Chiara Grappasonni, Giuliano Coppotelli, and D. J. Ewins. "Ground vibration tests of a helicopter structure using OMA techniques." *Mechanical Systems and Signal Processing* 35, no. 1-2 (2013): 35-51, https://doi.org/10.1016/j.ymssp.2012.09.013, (accessed on 20 July 2025).

9.　　Sibille, Luigi, Marco Civera, Luca Zanotti Fragonara, and Rosario Ceravolo. "Automated operational modal analysis of a helicopter blade with a density-based cluster algorithm." *AIAA Journal* 61, no. 3 (2023): 1411-1427, (accessed on 20 July 2025).

10.　　Češkovič, Marek, Martin Schrötter, Róbert Huňady, Pavol Kurdel, and Natália Gecejová. 2023. "Unwanted Supplementary Vibrations of Helicopter Radio Communication Systems" *Aerospace* 10, no. 7: 632. https://doi.org/10.3390/aerospace10070632 (accessed on 21 July 2025).

11. Tamer, Aykut, Andrea Zanoni, Alessandro Cocco, and Pierangelo Masarati. 2021. "A Generalized Index for the Assessment of Helicopter Pilot Vibration Exposure" *Vibration* 4, no. 1: 133-150. https://doi.org/10.3390/vibration4010012 (accessed on 21 July 2025).

12. Chiariello, Antonio, Carmine Carandente Tartaglia, Maurizio Arena, Vincenzo Quaranta, Giovanni Bruno, Marika Belardo, and Martina Castaldo. 2024. "Vibration Qualification Campaign on Main Landing Gear System for High-Speed Compound Helicopter" *Aerospace* 11, no. 2: 130. https://doi.org/10.3390/aerospace11020130 (accessed on 21 July 2025).

13. Yang, Renguo, Yadong Gao, Huaming Wang, and Xianping Ni. 2022. "Reducing Helicopter Vibration Loads by Individual Blade Control with Genetic Algorithm" *Machines* 10, no. 6: 479. https://doi.org/10.3390/machines10060479 (accessed on 21 July 2025).

14. Bertolino, Antonio Carlo, Matteo Gaidano, Stefano Smorto, Paolo Giovanni Porro, and Massimo Sorli. 2023. "Development of a High-Performance Low-Weight Hydraulic Damper for Active Vibration Control of the Main Rotor on Helicopters—Part 1: Design and Mathematical Model" *Aerospace* 10, no. 5: 391. https://doi.org/10.3390/aerospace10050391 (accessed on 21 July 2025).

15. Bertolino, Antonio Carlo, Matteo Gaidano, Stefano Smorto, Paolo Giovanni Porro, and Massimo Sorli. "Development of a High-Performance Low-Weight Hydraulic Damper for Active Vibration Control of the Main Rotor on Helicopters—Part 2: Preliminary Experimental Validation." *Aerospace* 10, no. 10 (2023): 868. (accessed on 21 July 2025).

16. Wang, Xiong, Changliang Lin, Wei Liu, Jinliang Wang, and Wenjie Wang. 2023. "A Topological Valley Stamping Plate for Low-Frequency-Vibration Isolation and Wave Manipulation in Helicopters" *Processes* 11, no. 10: 2941. https://doi.org/10.3390/pr11102941 (accessed on 21 July 2025).

17. Tamer, Aykut, Vincenzo Muscarello, Giuseppe Quaranta, and Pierangelo Masarati. 2020. "Cabin Layout Optimization for Vibration Hazard Reduction in Helicopter Emergency Medical Service" *Aerospace* 7, no. 5: 59. https://doi.org/10.3390/aerospace7050059 (accessed on 21 July 2025).

18. Feng, Yongqiang, Yaoxin Zheng, Luzhao Chen, Xiaodong Qu, and Guangyou Fang. 2022. "Method of Eliminating Helicopter Vibration Interference Magnetic Field with a Pair of Magnetometers" *Applied Sciences* 12, no. 4: 2065. https://doi.org/10.3390/app12042065 (accessed on 21 July 2025).

19. Bell UH-1 Iroquois, https://en.wikipedia.org/wiki/Bell_UH-1_Iroquois (accessed on 17 July 2025).

20. By Airwolfhound from Hertfordshire, UK - UH1 Huey - Fly Navy 2017, CC BY-SA 2.0, https://commons.wikimedia.org/w/index.php?curid=69215127, (accessed on 19 July 2025).

21. *Product Data: Piezoelectric Charge Accelerometer Types 4393 and 4393-V*. Copyright 2018-08 by Brüel & Kjaer. Downloaded from: https://www.bksv.com/media/doc/bp2043.pdf (accessed on 30 July 2023).

22. Bell UH-1H and UH-1C Iroquois (Huey), Pima Air and Space Museum, Tucson, Arizona, https://pimaair.org. Photo taken 24 July 2025.

23. Technical Documentation: Impact Hammer Type 8202. Copyright May, 1993 by Brüel & Kjaer. Available online: https://media. hbkworld.com/m/7a8ee3f9bea9db2b/original/Impact-Hammer-Type-8202.pdf (accessed on 30 July 2023).

24. Serridge, M.; Licht, T. *Piezoelectric Accelerometers and Vibration Preamplifiers: Theory and Application Handbook*; Brüel & Kjær: Naerum, Denmark, 1987. Available online: https://www.bksv.com/media/doc/bb0694.pdf (accessed on 30 July 2023).

25. Winarski, Daniel, Kip P. Nygren, and Tyson Winarski. 2023. "Modes of Vibration in Basketball Rims and Backboards and the Energy Rebound Testing Device" *Vibration* 6, no. 4: 726-742. https://doi.org/10.3390/vibration6040045. Available online: https://www.mdpi.com/2571-631X/6/4/45.

26. CATS: Computer Aided Test Suite Dynamic Control and Analysis STAR 7 Advanced Modal Analysis https://www.scribd.com/document/394925642/665498-MATERIJALI-1-Skripta-Listopad-2013, (accessed on 10 June 2023).

27. Blevins, Robert D. Formulas for Natural Frequency and Mode Shape, Reprinted 2001, Krieger Publishing, ISBN 1-57524-184-6, p. 108.

28. Yoo, H. H., and S. H. Shin. "Vibration analysis of rotating cantilever beams." *Journal of Sound and vibration* 212, no. 5 (1998): 807-828, https://dacemirror.sci-hub.box/journal-article/c37f6aa094b454e18b9a263bb0a3483e/yoo1998.pdf, (accessed on 1 August 2025).

29. Wright, A. D., C. E. Smith, R. W. Thresher, and J. L. C. Wang. "Vibration modes of centrifugally stiffened beams." (1982): 197-202, (accessed on 2 August 2025).

30. Lima, Marco António Costa Fonseca. "Rotating cantilever beams: Finite element modeling and vibration analysis." Master's thesis, Universidade do Porto (Portugal), 2012, (accessed on 4 August 2025).

31. STAR7 Operating Manual, Rev. 1b, Spectral Dynamics, Inc., San Jose, California. Supplied to STAR7 customers of Spectral Dynamics, (accessed on 10 June 2025).

32. Pastor, Miroslav, Michal Binda, and Tomáš Harčarik. "Modal assurance criterion." *Procedia Engineering* 48 (2012): 543-548, (accessed on 30 July 2025).

33. Winarski, T. Tsunami of Blockchain Technology and Patents: A Strategic Data Analytic Overview. *Jurimetr. J. Law Sci. Technol.* **2023**, *64*, 79–102, (accessed on 1 August 2025).